Control of low-frequency guided elastic wave modes in a hollow pipe using a meta-surface

A. Lalith Sai Srinivas Pillarisetti,[1] B. Cliff J Lissenden,[1] and C. Parisa Shokouhi[1, a)]

Department of Engineering Science and Mechanics, Penn State, University Park, Pennsylvania 16802, USA

(Dated: 16 July 2022)

A locally-resonant meta-surface for preferential excitation of a guided mode in a hollow pipe can improve ultrasonic guided wave inspection of pipelines. The proposed meta-surface comprises a periodic arrangement of bonded prismatic rod-like resonators in the circumferential and axial directions of the pipe. We demonstrate the presence of bandgaps for the low-frequency axisymmetric longitudinal modes L(0,1) and L(0,2), and the torsional mode T(0,1). The generated bandgaps can be exploited to filter higher harmonics associated with the system nonlinearity to improve nonlinear ultrasonic measurements on pipes. These bandgaps exist even for the non-axisymmetric flexural modes but with their hybridized dispersion curves exhibiting mode-coupling for higher circumferential orders. Moreover, a "partial" bandgap is obtained where preferential transmission of L(0,2) mode over L(0,1) is possible. We discuss the potential advantages of this partial bandgap to improve pipeline inspections using the L(0,2) mode. Time-domain finite element analyses are used to validate the presence of these bandgaps under the radial, circumferential and axial excitations that mimic the excitation using a ring of piezoelectric transducers. Finally, we discuss the influence of resonator spacing, filling fraction, and the number of resonator rings on the bandgaps for an informed meta-surface design.

[a)]shokouhi@psu.edu

I. INTRODUCTION

Ultrasonic guided wave inspection is a widely used technique for pipelines due to the ability of guided waves to travel long distances and their sensitivity to defects even at lower frequencies[1,2]. However, the tremendous potential of using guided modes in hollow pipes is often limited due to their multi-mode dispersive nature. The guided modes in pipes are classified into axisymmetric longitudinal modes L(0,n), axisymmetric torsional modes T(0,n), and non-axisymmetric flexural modes F(m,n), where m and n denote the circumferential order and the group number, respectively[3]. The low-frequency axisymmetric longitudinal modes, L(0,1) and L(0,2), and the torsional mode, T(0,1), are widely used for pipeline inspection, as they can be excited using a ring of ultrasonic transducers[4].

Among these axisymmetric modes, T(0,1) and L(0,2) are preferred due to their non-dispersive nature within a broad low-frequency range[5–11]. Moreover, neither mode has a radial displacement component responsible for leakage into fluids, and therefore they can travel long distances in fluid-filled pipes. In contrast, L(0,1) mode is dispersive and has particle motion in both radial and axial directions, and will dissipate energy in the presence of fluid. The L(0,2) mode is sometimes preferred over T(0,1) due to its higher group velocity, higher sensitivity to circumferential cracks, and lower attenuation in the presence of a viscoelastic coating[12]. Although the preferential excitation of T(0,1) mode is possible using a single circumferential ring of thickness-shear[13,14] or in-plane shear[15] piezoelectric transducers, the preferential excitation of L(0,2) mode requires multiple transducer (axially-polarized) rings to suppress the inherent L(0,1) mode excitation[16]. The particle motion of L(0,1) mode in the axial direction is responsible for its unavoidable excitation[17]. The presence of L(0,1) mode in inspections involving L(0,2) makes the signal processing complicated due to the unwanted mode conversions that result from L(0,1) mode interaction with defects[11],calling for new ways for preferential transmission of the L(0,2) mode using a single ring of transducers. On the other hand, a circumferential ring of radially-polarized transducers preferentially transmits L(0,1) mode, as L(0,2) mode has negligible radial particle motion[17]. The possible mode conversion of this preferentially excited L(0,1) mode to L(0,2) could enable L(0,2) mode pipeline inspections under a radial excitation of transducers, thereby reducing the complexity and cost of the transducer system.

Mode filtering also plays an important role in nonlinear ultrasonic guided wave measure-

ments for evaluating incipient damages. Li *et al.* demonstrated the use of the axisymmetric modes L(0,6) and L(0,10) as the fundamental and second harmonic wave modes, respectively, to measure the nonlinearity that arises from the changes in the microstructure due to thermal fatigue damage[18]. Choi *et al.* used third harmonics associated with T(0,1) mode to measure the fatigue damage in a Nickel alloy[19]. However, nonlinear measurements are extremely sensitive to the system nonlinearity arising from the actuation system such as the amplifiers, transducers and the ultrasonic couplant[20]. The presence of these inherent nonlinearities influence the amplitude of the higher harmonics which carry information about microstructural imperfections. Therefore, new techniques to suppress higher harmonics associated with the system nonlinearity is beneficial to nonlinear ultrasonic measurements.

Locally-resonant meta-surfaces have been proposed for structural inspection applications for mode filtering[21], mode conversion[22], steering[23], and focusing[24–26] of elastic waves in plates and pipes. Very recently, metamaterial-based filters for suppressing the higher harmonics associated with the system nonlinearity have been introduced[27–29]. The suppression is achieved by matching the second harmonic frequency with the bandgap frequency exhibited by the meta-material. The formation of bandgaps because of the hybridization of Lamb waves with different meta-surfaces was proposed for improving nonlinear ultrasonic measurements in plates[27,29]. However, bandgaps emerging from the hybridization between the guided modes in a pipe with meta-surfaces is not yet fully explored. Very recently, local resonance-based gradient index lenses were demonstrated to achieve the focusing of axisymmetric guided modes in pipes[25,26]. However, the application of meta-surfaces for preferential guided mode transmission and suppression in pipelines remains unexplored. In this paper, we demonstrate a meta-surface design with two important functional capabilities: (a) preferentially transmitting L(0,2) mode under radial and axial excitations, and (b) exhibiting bandgaps for axisymmetric and non-axisymmetric guided modes that can be exploited for improving nonlinear ultrasonic measurements.

The remainder of the paper is organized as follows. Section II discusses the hybridization between the axisymmetric and non-axisymmetric guided modes and the local resonances of prismatic rod-like resonators resulting in the generation of bandgaps. The time-domain finite element validation of the obtained bandgaps and the potential implications of the results are presented in Section III. The influence of resonator spacing, filling fraction and the number of resonator rings on the bandgaps is presented as a parametric study in Section IV. Finally,

we present key conclusions derived from our numerical studies in Section V that could potentially benefit the fields of nondestructive testing and structural health monitoring.

II. FORMATION OF BANDGAPS FOR AXISYMMETRIC AND NON-AXISYMMETRIC GUIDED MODES IN A HOLLOW PIPE

The proposed meta-surface comprises periodically stubbed prismatic rod-like resonators on a 4-inch profile (114.3 mm outer diameter and 6 mm thick) steel pipe (Fig. 1(a)). The unit cell considered is a 15 deg arc of the pipe (θ_s) including a steel resonator of dimensions 23mm × 8mm × 8mm (L × W × W), as shown in Fig. 1(a). The resonator dimensions are selected to attain a fixed-free longitudinal resonance frequency of the resonator around 50 kHz. The base of the resonator is slightly curved with a radius matching the outer radius of the pipe. A lattice length of a = 10 mm is considered along the axial direction. The defined sector angle (θ_s) and lattice length (a) imply an infinite array of resonator rings with 2 mm spacing in the axial direction with each ring comprising 24 ($\sim 360/15$) equally spaced resonators along the circumference. Imposing cyclic boundary conditions (BCs) to the pipe cross sections with normals oriented in the circumferential direction and Bloch Floquet BCs to the pipe cross sections with normals oriented in the axial direction enable selective generation of dispersion curves for any desired circumferential order m[30]. The hybridized dispersion curves for the guided modes propagating in the axial direction are then obtained through the eigenfrequency analysis in COMSOL Multiphysics software[31] by sweeping the Bloch wavenumber within the irreducible Brillouin zone.

The hybridized axisymmetric (m=0) dispersion curves in the presence of the meta-surface are shown in Fig. 1(b) for the desired low-frequency range. The hybridized modes are identified with respect to the unhybridized (without meta-surface) guided modes (L(0,n) and T(0,n)) by examining the modal vibrations exhibited by the pipe within the unit cell. For reference, the modal vibrations corresponding to the hybridized modes $L(0,1)_h$, $T(0,1)_h$, and $L(0,2)_h$ are shown in Figs 1(c), 1(d) and 1(e) at frequencies marked in Fig. 1(b). The hybridization between the axisymmetric guided modes (L(0,1), L(0,2) and T(0,1)) with the local resonances of the resonator is evident. The L(0,1) mode, having a predominant particle displacement in the radial direction, is observed to hybridize with the longitudinal resonance of the resonator (Fig. 1 (c)). This hybridization is akin to that observed for A0 Lamb wave

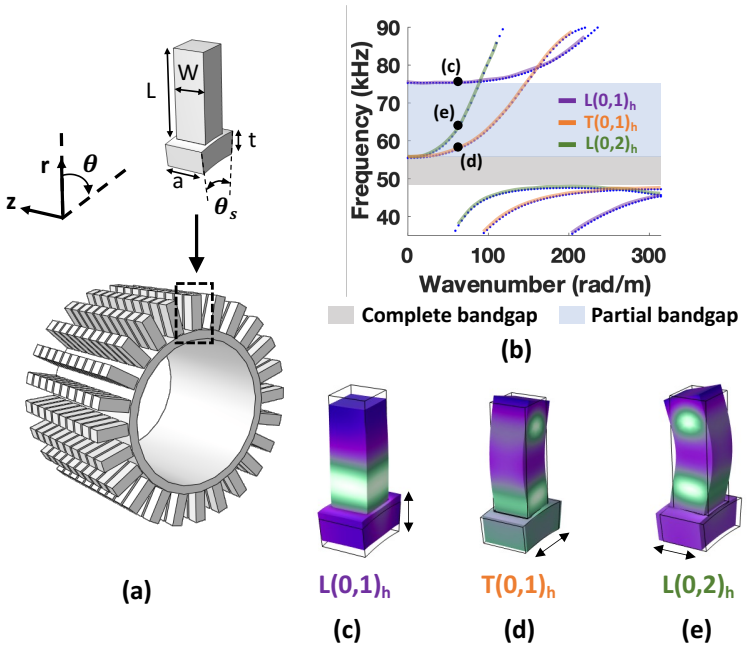

FIG. 1. (a) Schematic of the pipe with surface-mounted prismatic resonators and its corresponding unit cell. (b) Hybridized axisymmetric dispersion curves illustrating the complete and partial bandgaps. Mode shapes for the hybridized (c) L(0,1), (d) T(0,1), and (e) L(0,2) modes, at frequencies marked in (b).

mode in a plate under the presence of rod-like resonators[32,33]. In contrast, the T(0,1) and L(0,2) modes, having predominant particle displacement in the circumferential and axial directions, respectively, hybridize with the flexural resonances of the resonator (Figs. 1(d) and 1(e)). A bandgap from 47 kHz to 57 kHz is visible for all the possible axisymmetric modes (Fig. 1(b)), which we refer to as the "complete" bandgap. Moreover, we observe a range of frequencies above the complete bandgap where a bandgap for L(0,1) mode and a passband for L(0,2) mode coexist, and is hereafter referred to as the "partial" bandgap.

Next, we analyze the possible hybridizations between flexural modes (non-axisymmetric) and the meta-surface. The hybridized dispersion curves for the circumferential order (m) of 1, 2, 3 and 4 depict the presence of complete bandgap even for flexural modes (Figs. 2(a) - 2(d)). Moreover, mode coupling between the higher order circumferential modes at the crisscrossing of the dispersion curves is evident (Figs. 2(b) - 2(d)) similar to that observed for hybridized Lamb wave modes in plates with periodic stubs[34,35]. The dispersion curves at these crisscrossings repel to form a new set of individual dispersion curves, with

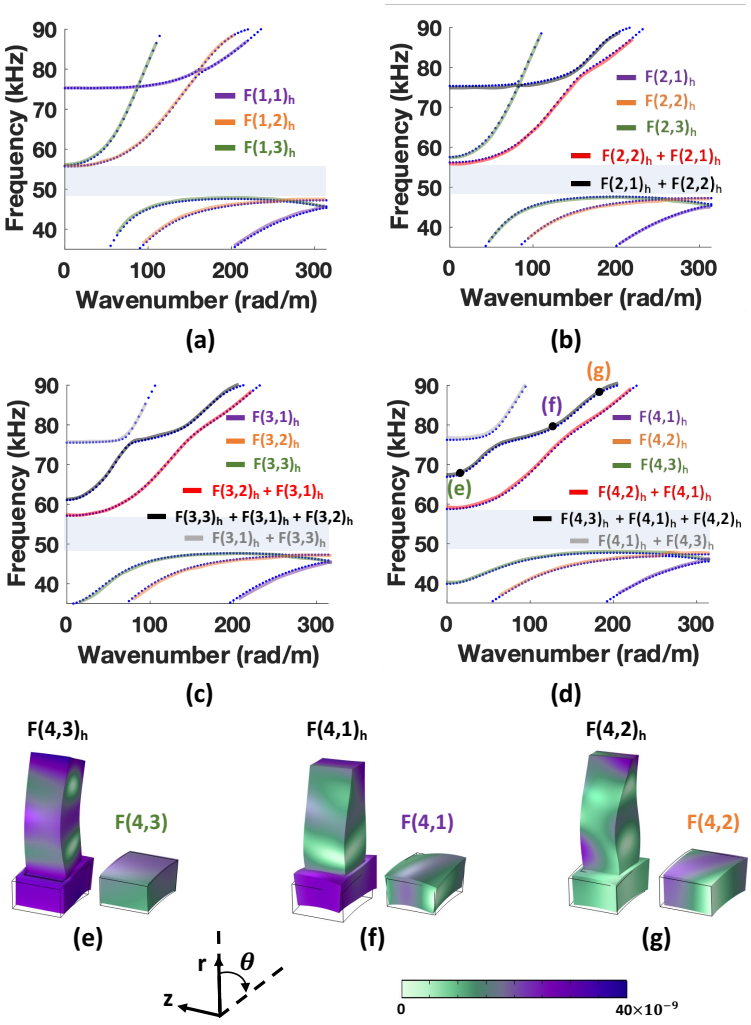

FIG. 2. Non-axisymmetric hybridized dispersion curves for the circumferential order of (a) m = 1, (b) m = 2, (c) m = 3, and (d) m = 4. Mode shapes corresponding to the hybridized (with meta-surface) and unhybridized (without meta-surface) flexural modes: (e) F(4,3), (f) F(4,1), and (g) F(4,2) modes, at frequencies marked in (d).

each curve possessing distinct guided modes. The observed mode coupling could be due to complex mode vibrations associated with the flexural modes having higher circumferential order. With an increase in the circumferential order, the flexural modes deviate from their axisymmetric counterparts resulting in non-intuitive hybridizations (see Figs. 2(e)-2(g)) with the local resonances of the resonators. To demonstrate this behaviour, the mode shapes at three distinct wavenumber-frequency pairs along a mode-coupled dispersion line (marked in Fig 2(d)) are depicted in Figs. 2(e)- 2(g) together with their unhybridized flexural mode counterparts. The local resonance-induced vibrations of the pipe at these three

wavenumber-frequency pairs match well with the corresponding unhybridized flexural modes (F(4,1), F(4,2), and F(4,3)) that propagate within the pipe, confirming the presence of mode-coupling. The presence of mode-coupling and complex local-resonance hybridizations makes it complicated to exploit the proposed meta-surface for preferential transmission/suppression of the flexural modes of higher circumferential order. We therefore restrict our analysis to axisymmetric modes and demonstrate the possible mode-filtering applications of the proposed meta-surface. In the subsequent sections, we numerically validate the presence of complete and partial bandgaps for axisymmetric modes and determine the possible mode-conversions that result from an incident axisymmetric guided mode at these bandgap frequencies.

III. NUMERICAL VALIDATION OF BANDGAPS

A. Complete bandgap

The presence of the complete bandgap is validated through the 3D time-domain finite element simulations in ABAQUS FEA software[36] on the pipe with the meta-surface comprising 10 resonator rings (Fig. 3(a)). The excitation is applied to 24 equally spaced points on the outer circumference of the pipe to preferentially excite axisymmetric modes, as shown in the schematic in Fig. 3(a). A 10-cycle Hanning windowed sinusoidal pulse at 51.5 kHz is used to study the interaction of axisymmetric modes (L(0,1), L(0,2) and T(0,1)) with the meta-surface within the complete bandgap frequency range. Absorbing layers with gradually increased damping (ALID) are used to prevent end-wall reflections of the axisymmetric modes[13,37]. The absorbing regions consist of 30 0.5-mm thick layers with mass damping coefficient in each layer following the cubic power law reaching a maximum of 7.5×10^5. The defined ALID layer sequence is able to significantly absorb the incident L(0,1), L(0,2) and T(0,1) modes for the desired frequency range (30-80 kHz). The time-domain simulations with excitations in radial, circumferential, and axial directions are performed to investigate the presence of the complete bandgap. The axial and circumferential displacement data are extracted and averaged over 24 equally spaced points on the pipe circumference at a 1 m distance from the meta-surface region in the incident (IR) and transmission (TR) regions (Fig. 3(a)).

Figs. 3(b) and 3(f) depict the averaged axial displacement extracted in the incident

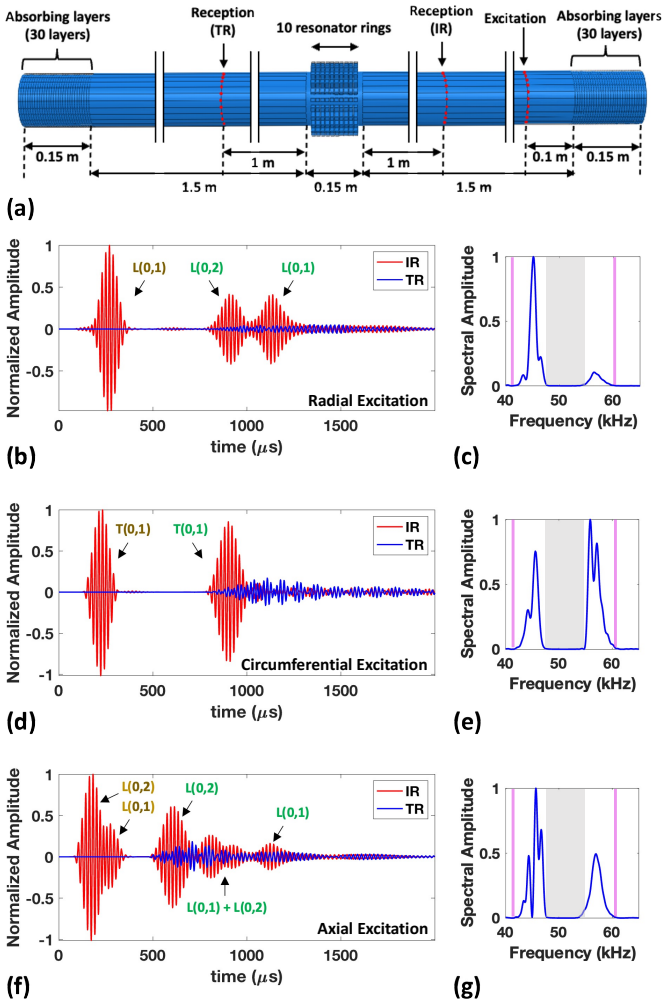

FIG. 3. (a) The finite element model of the pipe with the meta-surface comprising 10 resonator rings (24 resonators in each ring). The axial displacement data are averaged over 24 reception points in the incident (IR) and transmission regions (TR) for the (b) radial and (f) axial excitations at a frequency (51.5 kHz) falling within the complete bandgap. The circumferential displacement data averaged over 24 reception points in the incident (IR) and transmission regions (TR) for the (d) circumferential excitation at a complete bandgap frequency. The frequency spectra of the displacement data received in the transmission region (TR) are shown for the (c) radial, (e) circumferential and (g) axial excitations. The incident and reflected wave modes are identified and colored in brown and green, respectively, in plots (b), (d) and (f). Highlighted in grey in (c), (e) and (g) are the complete bandgaps obtained from the eigenfrequency analysis and the frequency-bounds of the incident tone-burst are marked in pink.

and transmission regions for the radial and axial excitations, respectively, whereas Fig 3(d) depicts the circumferential displacement extracted in the incident and transmission regions for the circumferential excitation. The wave packets received in the incident region (IR) before 500 μs in all the displacement plots (Figs. 3(b), 3(d), and 3(f)) correspond to the incident guided modes propagating towards the meta-surface. As expected, the radial and circumferential excitations of a pipe results in the preferential transmission of L(0,1) mode and T(0,1) mode, respectively (Figs. 3(b) and 3(d)). In contrast, the axial excitation results in the excitation of both L(0,2) and L(0,1) modes.

When excited at the frequencies within the bounds of the complete bandgap, the L(0,1) and L(0,2) modes incident on the meta-surface result in the reflection and mode-conversion to L(0,1) and L(0,2) modes, indicating the presence of a bandgap for both these modes (Figs. 3(b) and 3(f)). On the other hand, the incident T(0,1) mode is predominantly reflected without any mode conversion (Fig. 3(d)), possibly because of the absence of higher-order axisymmetric torsional modes at the incident frequency. The low-amplitude wave packets observed beyond the meta-surface in the transmission region (TR) for all the excitation types correspond to the wave packets with frequencies outside the complete bandgap. Analyzing the frequency spectrum of these low-amplitude transmitted wave packets corroborates the presence of a complete bandgap, as evidenced from the dispersion analysis earlier (Figs. 3(c), 3(e), and 3(g)). In terms of potential implications of these results, the existence of a complete bandgap enables suppression of higher harmonics associated with system nonlinearity, i.e., matching the second harmonic frequency of the excited L(0,1) or L(0,2) or T(0,1) modes with the complete bandgap frequency can improve nonlinear ultrasonic measurements in pipes, as recently demonstrated for plates[27,28].

B. Partial bandgap

The efficiency of the meta-surface for the preferential transmission of L(0,2) mode is validated using the same finite element model shown in Fig. 3(a), but this time for axial and radial excitations at the partial bandgap frequency of 65 kHz. In the case of axial excitation, we observe a significant transmission and reflection of the incident L(0,2) and L(0,1) modes, respectively, as expected because of the partial bandgap (Figs. 4(a) and (b)). However, there exists unavoidable mode-conversions (L(0,1) to L(0,2) and L(0,2) to L(0,1))

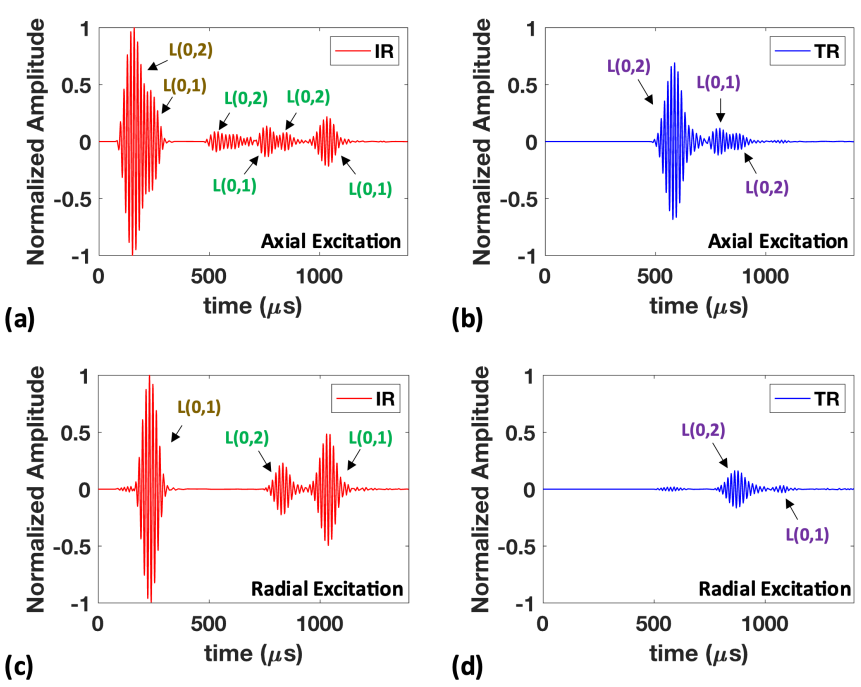

FIG. 4. The axial displacement data averaged over 24 reception points in the (a) incident (IR) and (b) transmission regions (TR) for the axial excitation at a partial bandgap frequency. The axial displacement data averaged over 24 reception points in the (c) incident (IR) and (d) transmission regions (TR) for the radial excitation at a partial bandgap frequency. The wave modes that are incident, reflected, and transmitted are identified and color coded in brown, green, and purple, respectively.

from the incident modes which transmit beyond the meta-surface (Fig. 4(b)). Nonetheless, the amplitudes of these mode-converted wave packets are significantly smaller (by a factor of 6) compared to the preferentially transmitted L(0,2) wave packet. These simulation results demonstrate the potential of the proposed meta-surface for L(0,2) mode pipe inspections using just a single ring of piezoelectric transducers, in contrast to the general requirement of multiple rings to suppress the excited L(0,1) mode[16].

In the case of radial excitation, which preferentially excites a pure L(0,1) mode, we observe a significant reflection of L(0,1) and mode-converted L(0,2) modes, as expected because of the partial bandgap (Fig. 4(c)). We also see a transmission of a low-amplitude mode-converted L(0,2) mode beyond the meta-surface (Fig. 4(d)). The amplitude of this transmitted L(0,2) wave packet can be increased by increasing the amplitude of the incident L(0,1) wave. The

other mode-converted transmitted modes are significantly smaller (5.5 times) compared to the preferentially transmitted L(0,2) mode (Fig. 4(d)). These simulation results demonstrate the efficiency of the proposed meta-surface for L(0,2) mode pipe inspections using a single ring of compressional piezoelectric transducers, significantly reducing the weight and cost of the transducer system[17]. The presence of the transmitted low-amplitude mode converted L(0,2) mode under radial excitation makes it impractical to exploit the partial bandgap frequency range to completely suppress the system-generated higher harmonics associated with the incident L(0,1) mode. Therefore, the possible use of the proposed meta-surface for nonlinear ultrasonic inspections is restricted within the complete bandgap frequency range, where neither of the axisymmetric modes can propagate, whereas the partial bandgap frequency range can be exploited for preferential transmission of L(0,2) mode under radial and axial excitations. Further optimization of the meta-surface design is required to obtain wider bandgaps with a minimum number of resonators. In the subsequent section we discuss the influence of resonator spacing, filing fraction, and the number of resonator rings on the bandgaps for an informed meta-surface design.

IV. PARAMETRIC STUDY

A parametric study is performed to analyze the partial and complete bandgaps by varying the sector angle (θ_s = 12°, 15°, 18°, 20°, 24°, a = 10 mm, W = 8 mm), lattice length in the axial direction (a = 10, 11, 12, 13, 14, 15, 16, θ_s = 15°, W = 8 mm), and the resonator width (W = 3, 4, 5, 6, 7, 8, θ_s = 15°, a = 10 mm). It is important to note that the combination of sector angle, lattice length, and resonator width determine the number of resonators in the circumferential direction ($360/\theta_s \sim$ 30 to 12), resonator spacing in the axial direction (a-W $\sim$ 2 mm to 8 mm), and filling fraction of the unit cell ($W^2/(r\theta_s a) \sim$ 0.06 to 0.42), respectively.

The hybridized dispersion curves are analyzed for each of the above cases, with the positioning and width of complete and partial bandgaps illustrated in Fig. 5. With an increase in the sector angle, both the partial and complete bandgaps are observed to shrink (Fig. 5(a)), whereas increasing the lattice length has limited influence over the bandgap widths (Fig. 5(b)). Varying the resonator width influences the positioning of flexural frequencies and therefore affects the bandgap positioning and width (Fig. 5(c)). However, we still observe

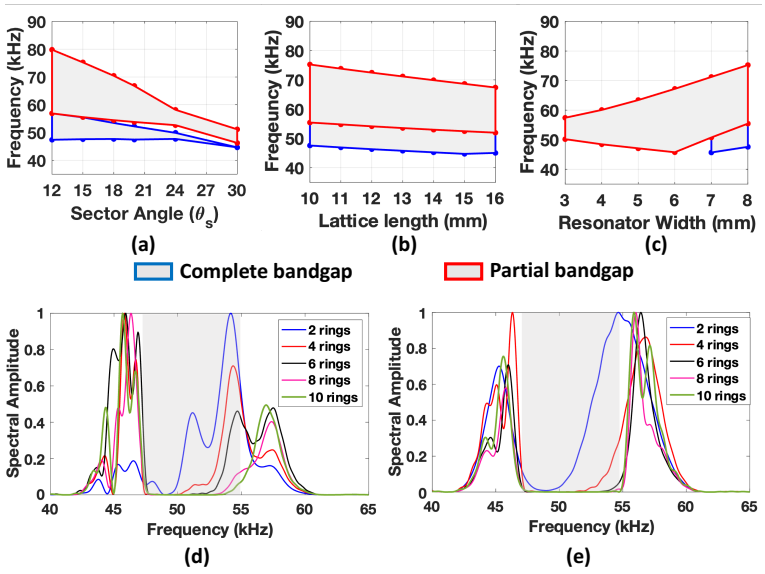

FIG. 5. Influence of (a) sector angle, (b) lattice length, and (c) resonator width on the positioning and width of complete and partial bandgaps. The influence of the number of resonator rings in the meta-surface on the frequency spectra of the (d) axial and (e) circumferential displacement data received in the transmission region (TR) under the axial and circumferential excitations, respectively. Highlighted in grey in (d) and (e) are the complete bandgaps obtained from the eigenfrequency analysis.

the presence of a partial bandgap over all the resonator widths, with complete bandgaps observed only for a higher filling fraction. To further inform the meta-surface design, the minimum number of resonator rings required to achieve the bandgap should be investigated. Figs. 5(d) and (e) depict the frequency spectrum of the transmitted wave packets beyond the meta-surface ($\theta_s = 15$, a = 10, W = 8) while varying the number of resonator rings for axial (excites both L(0,1) and L(0,2)) and circumferential (excites T(0,1)) excitations within the complete bandgap frequency (51.5 kHz), similar to that previously shown in Figs. 2(c), 2(e) and 2(g). Fig. 5(d) suggests that at least 8 resonator rings are required to match the bandgap (for L(0,1) and L(0,2)) from the time-domain simulation to that obtained for an infinite array of resonators using eigenfrequency analysis. In contrast, matching the T(0,1) bandgap requires a minimum of 6 resonator rings (Fig. 5(e)).

V. CONCLUSION

We address the feasibility of a meta-surface comprising prismatic resonators for controlling guided-mode propagation in a pipe. We demonstrated the existence of complete bandgaps for L(0,1), T(0,1), and L(0,2) modes using the eigenfrequency analysis and time domain finite-element analysis that can be leveraged for higher harmonic filtering to improve nonlinear ultrasonic measurements. The presence of complete bandgaps and mode-coupling for flexural modes of higher circumferential order is illustrated. The axisymmetric hybridized dispersion curves exhibit a frequency range which is a passband for L(0,2) mode while forbidding L(0,1) mode. Leveraging this partial bandgap, we can improve L(0,2) mode pipe inspections by reducing the cost and complexity of the transducer system. The sensitivity of the bandgaps to various design parameters is analyzed to inform an optimized meta-surface design for experimental validation. This work provides insight into the hybridizations between the guided modes in a hollow pipe and local resonances of a prismatic resonator, which could be leveraged to address some of the challenges of linear and nonlinear ultrasonic guided wave pipeline inspections.

ACKNOWLEDGMENTS

The authors gratefully acknowledge the support of the National Science Foundation under Grant No. 1934527. Any opinions, findings, and conclusions or recommendations expressed in this material are those of the author(s) and do not necessarily reflect the views of the National Science Foundation.

Computations for this research were performed on the Pennsylvania State University's Institute for Computational and Data Sciences' Roar supercomputer.

DATA AVAILABILITY STATEMENT

The data that support the findings of this study are available from the corresponding author upon reasonable request.

REFERENCES

[1]J. L. Rose, *Ultrasonic guided waves in solid media* (Cambridge university press, 2014).

[2]M. Mitra and S. Gopalakrishnan, "Guided wave based structural health monitoring: A review," Smart Materials and Structures **25**, 053001 (2016).

[3]M. Silk and K. Bainton, "The propagation in metal tubing of ultrasonic wave modes equivalent to lamb waves," Ultrasonics **17**, 11–19 (1979).

[4]A. Ghavamian, F. Mustapha, B. Baharudin, and N. Yidris, "Detection, localisation and assessment of defects in pipes using guided wave techniques: a review," Sensors **18**, 4470 (2018).

[5]A. Demma, P. Cawley, M. Lowe, and A. Roosenbrand, "The reflection of the fundamental torsional mode from cracks and notches in pipes," The Journal of the Acoustical Society of America **114**, 611–625 (2003).

[6]Z. Liu, C. He, B. Wu, X. Wang, and S. Yang, "Circumferential and longitudinal defect detection using t (0, 1) mode excited by thickness shear mode piezoelectric elements," Ultrasonics **44**, e1135–e1138 (2006).

[7]N. Nakamura, H. Ogi, and M. Hirao, "Mode conversion and total reflection of torsional waves for pipe inspection," Japanese Journal of Applied Physics **52**, 07HC14 (2013).

[8]M. J. Lowe, D. N. Alleyne, and P. Cawley, "Defect detection in pipes using guided waves," Ultrasonics **36**, 147–154 (1998).

[9]D. Alleyne and P. Cawley, "The long range detection of corrosion in pipes using lamb waves," in *Review of progress in quantitative nondestructive evaluation* (Springer, 1995) pp. 2073–2080.

[10]D. Alleyne and P. Cawley, "The effect of discontinuities on the long-range propagation of lamb waves in pipes," Proceedings of the Institution of Mechanical Engineers, Part E: Journal of Process Mechanical Engineering **210**, 217–226 (1996).

[11]D. Alleyne and P. Cawley, "The excitation of lamb waves in pipes using dry-coupled piezoelectric transducers," Journal of Nondestructive Evaluation **15**, 11–20 (1996).

[12]D. Alleyne, T. Vogt, and P. Cawley, "The choice of torsional or longitudinal excitation in guided wave pipe inspection," Insight-Non-Destructive Testing and Condition Monitoring **51**, 373–377 (2009).

[13]X. Niu, W. Duan, H.-P. Chen, and H. Marques, "Excitation and propagation of torsional t (0, 1) mode for guided wave testing of pipeline integrity," Measurement **131**, 341–348 (2019).

[14]H. Miao, Q. Huan, Q. Wang, and F. Li, "Excitation and reception of single torsional wave t (0, 1) mode in pipes using face-shear d24 piezoelectric ring array," Smart Materials and Structures **26**, 025021 (2017).

[15]W. Zhou, F.-G. Yuan, and T. Shi, "Guided torsional wave generation of a linear in-plane shear piezoelectric array in metallic pipes," Ultrasonics **65**, 69–77 (2016).

[16]D. Alleyne, B. Pavlakovic, M. Lowe, and P. Cawley, "Rapid, long range inspection of chemical plant pipework using guided waves," in *AIP conference proceedings*, Vol. 557 (American Institute of Physics, 2001) pp. 180–187.

[17]P. Lowe, R. Sanderson, S. Pedram, N. Boulgouris, and P. Mudge, "Inspection of pipelines using the first longitudinal guided wave mode," Physics Procedia **70**, 338–342 (2015).

[18]W. Li and Y. Cho, "Thermal fatigue damage assessment in an isotropic pipe using nonlinear ultrasonic guided waves," Experimental Mechanics **54**, 1309–1318 (2014).

[19]G. Choi, Y. Liu, and C. J. Lissenden, "Nonlinear guided waves for monitoring microstructural changes in metal structures," in *Pressure Vessels and Piping Conference*, Vol. 57021 (American Society of Mechanical Engineers, 2015) p. V007T07A002.

[20]C. J. Lissenden, "Nonlinear ultrasonic guided waves—principles for nondestructive evaluation," Journal of Applied Physics **129**, 021101 (2021).

[21]W. Wang, B. Bonello, B. Djafari-Rouhani, Y. Pennec, and J. Zhao, "Elastic stubbed metamaterial plate with torsional resonances," Ultrasonics **106**, 106142 (2020).

[22]Y. Tian, Y. Song, Y. Shen, and Z. Yu, "A metamaterial ultrasound mode convertor for complete transformation of lamb waves into shear horizontal waves," Ultrasonics **119**, 106627 (2022).

[23]H. Zhu and F. Semperlotti, "Anomalous refraction of acoustic guided waves in solids with geometrically tapered metasurfaces," Physical review letters **117**, 034302 (2016).

[24]X. Yan, R. Zhu, G. Huang, and F.-G. Yuan, "Focusing guided waves using surface bonded elastic metamaterials," Applied Physics Letters **103**, 121901 (2013).

[25]G. Okudan, H. Danawe, D. Ozevin, and S. Tol, "Torsional wave focusing in cylindrical structures with the conformal gradient-index phononic crystal lens," Journal of Applied Physics **129**, 174902 (2021).

[26]H. Danawe, G. Okudan, D. Ozevin, and S. Tol, "Conformal gradient-index phononic crystal lens for ultrasonic wave focusing in pipe-like structures," Applied Physics Letters **117**, 021906 (2020).

[27]Y. Tian, Y. Shen, D. Rao, and W. Xu, "Metamaterial improved nonlinear ultrasonics for fatigue damage detection," Smart Materials and Structures **28**, 075038 (2019).

[28]K. VK, K. Balasubramaniam, and P. Rajagopal, "Waveguide metamaterial rod as mechanical acoustic filter for enhancing nonlinear ultrasonic detection," APL Materials **9**, 061115 (2021).

[29]S. Shan, F. Wen, and L. Cheng, "Purified nonlinear guided waves through a metamaterial filter for inspection of material microstructural changes," Smart Materials and Structures **30**, 095017 (2021).

[30]C. Hakoda, J. Rose, P. Shokouhi, and C. Lissenden, "Using floquet periodicity to easily calculate dispersion curves and wave structures of homogeneous waveguides," in *AIP Conference Proceedings*, Vol. 1949 (AIP Publishing LLC, 2018) p. 020016.

[31]COMSOL Multiphysics, "User's manual version 5.6," COMSOL Inc (2020).

[32]M. Rupin, F. Lemoult, G. Lerosey, and P. Roux, "Experimental demonstration of ordered and disordered multiresonant metamaterials for lamb waves," Physical review letters **112**, 234301 (2014).

[33]E. G. Williams, P. Roux, M. Rupin, and W. Kuperman, "Theory of multiresonant metamaterials for a 0 lamb waves," Physical Review B **91**, 104307 (2015).

[34]T.-T. Wu, Z.-G. Huang, T.-C. Tsai, and T.-C. Wu, "Evidence of complete band gap and resonances in a plate with periodic stubbed surface," Applied Physics Letters **93**, 111902 (2008).

[35]T.-C. Wu, T.-T. Wu, and J.-C. Hsu, "Waveguiding and frequency selection of lamb waves in a plate with a periodic stubbed surface," Physical Review B **79**, 104306 (2009).

[36]Abaqus/CAE User's Guide Version 6.13, "User's manual version 5.6," Dassault Systèmes Simulia Corp (2018).

[37]P. Rajagopal, M. Drozdz, E. A. Skelton, M. J. Lowe, and R. V. Craster, "On the use of absorbing layers to simulate the propagation of elastic waves in unbounded isotropic media using commercially available finite element packages," Ndt & e international **51**, 30–40 (2012).